Physica Scripta

PAPER

The absorption properties of one-dimensional spherical photonic crystals based on plasma material

RECEIVED
8 December 2022

REVISED
31 December 2022

ACCEPTED FOR PUBLICATION
22 March 2023

PUBLISHED
31 March 2023

Tianqi Zhu[1], **You Lv**[1], **Ziran Wang**[2] **and Haifeng Zhang**[1,*]

[1] College of Electronic and Optical Engineering & College of Flexible Electronics (Future Technology), Nanjing University of Posts and Telecommunications, Nanjing 210023, People's Republic of China
[2] College of Telecommunications & Information Engineering, Nanjing University of Posts and Telecommunications, Nanjing 210023, People's Republic of China
[*] Author to whom any correspondence should be addressed.

E-mail: hanlor@163.com

Keywords: spherical photonic crystals, plasma material, absorption, transfer matrix method

Abstract

The first theoretical treatment of the electromagnetic properties of one-dimensional plasma spherical photonic crystals (1D PSPCs) in the non-magnetized state is carried out to obtain the expressions for the electric and magnetic fields. The utilization of the transfer matrix method provides a new idea for the exploration of the 1D PSPCs, based on which the expressions for the absorptance of the 1D PSPCs are derived. A structure of quasi-periodic 1D PSPCs arranged according to the Thue-Morse sequence is proposed to acquire the ultra-wide absorption bands (ABs) at large incidence angles by adding an air layer and setting the plasma frequency in a gradient. And the factors affecting the ABs are meticulously analyzed. It is figured out that the primary factors affecting ABs are topology and plasma frequency, both of which have vigoroso influences on the bandwidths and positions of ABs. However, the initial radius and the collision frequency prevailingly affect the amplitude of the absorptance. The unexceptionable geometric properties of the 1D PSPCs make them sensitive to parameter changes and can be applied in the field of absorbers and radomes, which have great application prospects and development space.

1. Introduction

Since the concept of photonic crystals (PCs) was introduced by two pioneers, Yablonovitch and John [1, 2], PCs are favored by domestic and foreign researchers for their good optical properties and are of tremendous value in the field of optics [3, 4], electromagnetics [5] and device design such as sensors [6] and optical multiplexers [7]. The theoretical study of PCs also continues to advance, and Pendry *et al* developed the transfer matrix method (TMM) [8, 9], which finitely differentiates Maxwell's equations in real space, allowing the distribution of the incident field to be found on the premise that the distribution of the incident field in the initial layer is known, enriching the way of solving the transmission properties of PCs. Guided by the correct theory, the studies of PCs have achieved world-renowned accomplishments.

PCs have multiple morphologies, and Li *et al* have systematically investigated the transmission properties of the one-dimensional (1D) planar photonic crystals (PPCs) employing TMM [10]. Inspired by the 1D PPCs, investigations of the 1D cylindrical photonic crystals (CPCs) have been on the agenda. Hu and other scientists have pioneered and consummated the theory of transmission properties and dispersion relationships of the 1D CPCs [11–13], which is momentous for fiber preparation [14] and sensor development [15]. The predominant optical properties of the 1D CPCs have provided new ideas for the development of PCs, and researchers shifted their attention to spheres possessing better geometric symmetry and engaged in working on the study of the 1D spherical photonic crystals (SPCs). Santiago *et al* carried out an in-depth analysis concerning the rationale of the spherical wave function and refined the decomposition method of the spherical wave function for scattered electromagnetic fields under general dielectric surfaces [16]. In 2016, Wendel and his colleagues solved the

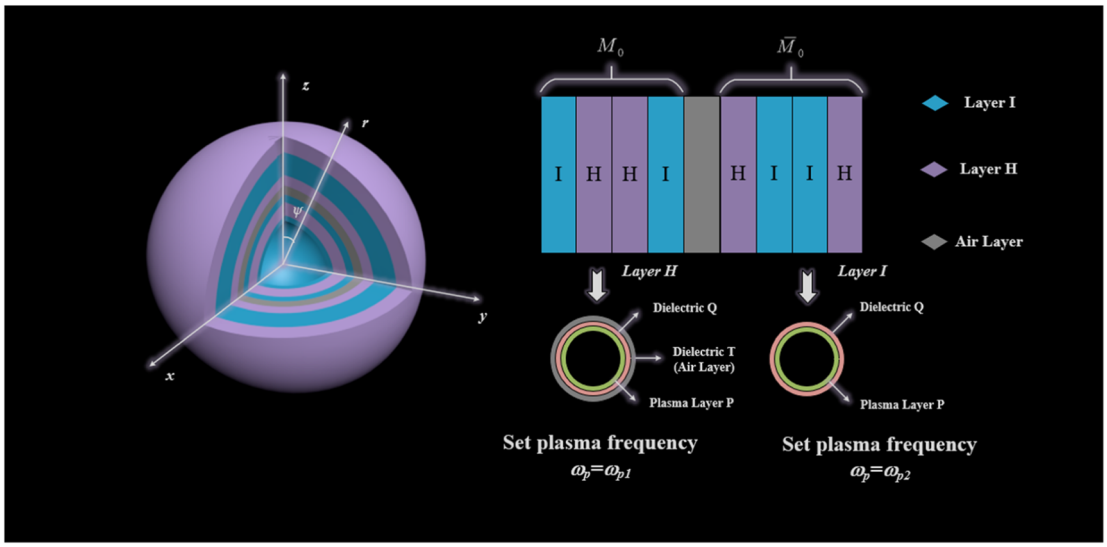

Figure 1. The schematic diagram of the structure of 1D PSPCs employing the Thue-Morse sequence.

propagation of arbitrary incident waves by eliminating the prefactor of the radial spherical Bessel functions [17]. The 1D SPCs have enormous potential for applications in nano [18], electronic communication [19], chemical [20], and sensor [21] fields up till the present moment.

Plasma possesses unique magneto-optical effects and absorption properties, which in combination with PCs can be utilized to design tunable and reconfigurable microwave devices with substantial value. The concept of the 1D magnetized plasma photonic crystals (MPPCs) was first proposed by Hojo and Mase, who gave a dispersion relation equation for the 1D MPPCs and analyzed it theoretically [22]. In 2010, Qi *et al* explored the electromagnetic properties of 1D MPPCs via the TMM and profoundly discussed the effects of the plasma parameters on transmission properties, filling a gap in the theory of 1D MPPCs [23]. Simultaneously, as the research on PCs continues to intensify, quasi-periodic PCs with different optical properties from those of periodically aligned PCs are widely applied by researchers, providing new directions for the development of thermal emitter devices [24], inverters [25], polarization selectors [26] and absorbers [27–29]. Intending to further improve the performance of PCs, Wang *et al* employed the Thue-Morse sequence in the 1D CPCs and investigated their nonreciprocal features [30]. This leads us to wonder whether 1D plasma spherical photonic crystals (PSPCs) with the most splendid geometrical shape can exhibit excellent electromagnetic properties in quasi-periodic arrangements, but there are infrequent studies and applications for 1D PSPCs in the current time frame, and there is a prodigious theoretical gap.

In this paper, the TMM is used to obtain the expressions for the absorptance of 1D PSPCs without the influences of the magnetic field. Meanwhile, after adequately comparing the quasi-periodic sequences such as periodic arrangement, Pell sequence [31], and Fibonacci sequence [32], the 1D quasi-periodic PSPCs based on the Thue-Morse sequence are constructed, and the effects of plasma frequency, collision frequency, initial radius, incident angle and arrangement on the absorptance of the 1D PSPCs are discussed in detail. This eradicates obstacles to the design of spherical multifunctional absorbers and antenna protection devices. In particular, 1D PSPCs are still in the theoretical stage, and the specific implementation is currently under further exploration.

2. Simulation model and formulation

The structure of the 1D PSPCs is depicted in figure 1, which adopts the Thue-Morse sequence. According to the basic knowledge of Thue-Morse sequence, the structure should be arranged in the following form [30].

$$M_k = M_{k-1}\bar{M}_{k-1}(k \geqslant 1) \tag{1}$$

$\bar{M}_{k-1}$ is the complement part of $\bar{M}_{k-1}$, and

$$M_0 = \{IHHI\},\ \bar{M}_0 = \{HIIH\} \tag{2}$$

Thereinto, the H layer consists of the general dielectric Q, the general dielectric T, and plasma layer P and the I layer is composed of dielectric Q and plasma layer P. The detailed arrangement of the I and H layers is shown in figure 1. Normalize d so that $d = 1$, the initial radius r_0 is d, the thickness d_Q of the general dielectric Q is $0.2d$, the

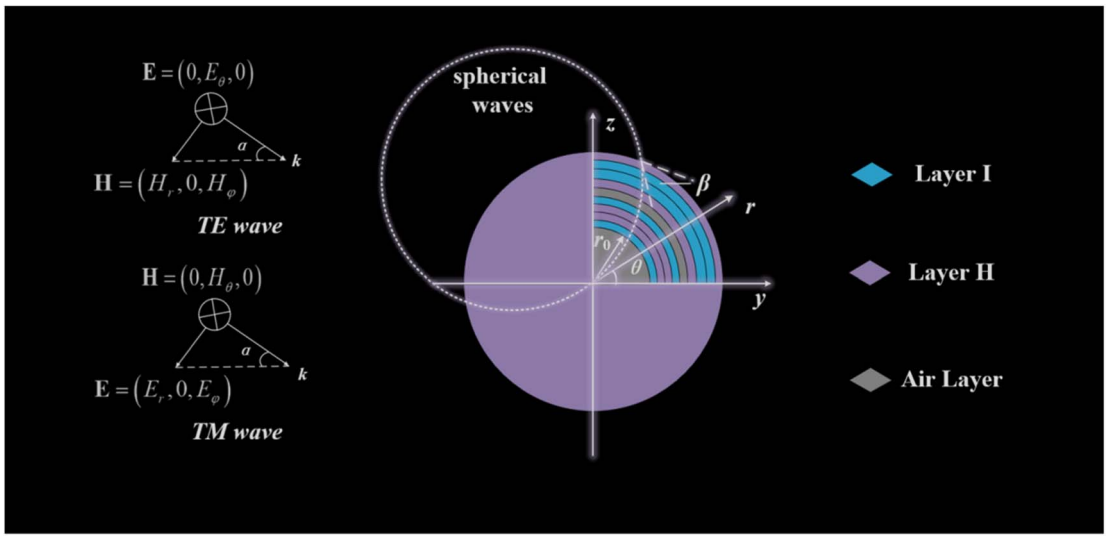

Figure 2. The main view of the 1D PSPCs with the Thue-Morse sequence applied and incidence angle marked.

thickness d_T of the general dielectric T is $0.25d$, and the thickness d_P of the plasma P is $0.55d$. Also, to improve the stability of the absorption band, an air layer with a thickness of $0.4d$ is added after M_0. The refractive index of the general dielectric Q is $n_Q = 2.8$, the refractive index of the general dielectric T is $n_T = 1$, and the effective magnetic permeability of the plasma layer P will be described in detail below.

Referring to the definition of TE and TM modes in the cylindrical plane coordinate system, it is undemanding to be conscious that the electric field $\boldsymbol{E}$ takes the form of $E = (0,\ E_\theta,\ 0)$ and the magnetic field $\boldsymbol{H}$ takes the form of $H = (H_r,\ 0,\ H_\varphi)$ in the TE waves. Homoplastically, in the TM waves, the electric field $\boldsymbol{E}$ is denoted as $E = (E_r,\ 0,\ E_\varphi)$ and the magnetic field $\boldsymbol{H}$ (see figure 2) is denoted as $H = (0,\ H_\theta,\ 0)$. Due to the special geometric properties of the spherical surface, the definition of the incidence angle of 1D PSPCs is quite distinguishable from that of 1D CPCs and 1D PPCs. Starting from the intersection of the 1D PSPCs and the spherical wave, tangents are made to the 1D PSPCs and the spherical waves, respectively, and the angle between the two tangents is the angle of incidence. The electromagnetic wave is incident from the *yoz* plane at an angle β to the plane. Under TE polarization, the wave vector $\boldsymbol{k}$ is always perpendicular to the magnetic field $\boldsymbol{H}$. Under TM polarization, the electric field $\boldsymbol{E}$ is always perpendicular to the wave vector $\boldsymbol{k}$.

The set of Maxwell's equations applicable to the non-magnetized plasma is as follows [32]:

$$\nabla \times \mathbf{E} = -\mu_0 \frac{\partial \mathbf{H}}{\partial t} \tag{3}$$

$$\nabla \times \mathbf{H} = \varepsilon_0 \frac{\partial \mathbf{E}}{\partial t} + \mathbf{J} \tag{4}$$

$$\frac{d\mathbf{J}}{dt} + \nu_c \mathbf{J} = \varepsilon_0 \omega_p^2 \mathbf{E} \tag{5}$$

where J is a vector quantity, called polarization current density, which can be decomposed along the three directions r, θ, and ψ. ν_c is the collision frequency and ω_p is the plasma frequency. ω_c is the cyclotron frequency of the plasma, denoted as $eB_0/m\mathbf{e_\theta}$.

By taking into account the relationship between **J** and **E**, in the non-magnetized plasma layer, equation (2) can be rewritten as [32]:

$$\nabla \times \mathbf{H} = \varepsilon_0 \varepsilon_p \frac{\partial \mathbf{E}}{\partial t} \tag{6}$$

here,

$$\varepsilon_p = 1 - \frac{\omega_p^2}{\omega(\omega + i\nu_c)} \tag{7}$$

Under the TM waves, the electric and magnetic fields are represented as:

$$E = e^{-i\omega t}(E_r,\ 0,\ E_\varphi) \tag{8}$$

$$H = e^{-i\omega t}(0,\ H_\theta,\ 0) \tag{9}$$

Decomposing equations (3) and (4) in $\boldsymbol{r}$, θ, and $\boldsymbol{\psi}$ directions and incorporating the transmission properties of spherical waves, the derivative of $\boldsymbol{\psi}$ can be omitted.

$$\frac{1}{r^2 \sin\theta}\left[-\frac{\partial}{\partial\varphi}(rH_\theta)\right] = i\omega\varepsilon_0(\varepsilon_1 E_r + i\varepsilon_2 E_\varphi) \tag{10a}$$

$$\frac{1}{r}\left[\frac{\partial}{\partial r}(rH_\theta)\right] = i\omega\varepsilon_0(-i\varepsilon_2 E_r + \varepsilon_1 E_\varphi) \tag{10b}$$

where ε_1 denotes the dielectric constant of the incident layer and ε_2 represents the dielectric constant of the emitted layer.

Synthesizing the above equations, the following results can be generated.

$$\frac{1}{r^2}\frac{\partial}{\partial r}\left(r^2\frac{\partial H_\theta}{\partial r}\right) + \frac{1}{r^2\sin^2\theta}\frac{\partial^2 H_\theta}{\partial\varphi^2} + k^2 H_\theta = 0 \tag{11}$$

In addition, here $k = \omega\cos\beta\sqrt{\mu_0\varepsilon_0\varepsilon_{TM}}$, $\varepsilon_{TM} = (\varepsilon_1^2 - \varepsilon_2^2)/\varepsilon_1$ and β is the incident angle. In the following, define $H_\theta(x,\ \varphi) = V(x)\Psi(\varphi)$,where $x = kr$. Readily-easily know the angular part of $H\theta$ satisfies the following equation.

$$\frac{d^2\Psi}{d\varphi^2} + m^2\varphi = 0 \tag{12}$$

With the intention of constructing the spherical Bessel equation and obtain the solutions for the magnetic and electric fields, in the first place let,

$$m^2 = l(l+1)\sin^2\theta \tag{13}$$

Then combining equations (9), (10) and (11), the spherical Bessel equation for the magnetic field $H\theta$ can be accessed.

$$x^2\frac{d^2V}{dx^2} + x\frac{dV}{dx} + \left[x^2 - \left(l+\frac{1}{2}\right)^2\right]V(x) = 0 \tag{14}$$

In accordance with the knowledge of the spherical Bessel equation, it is well known that the solution of the Bessel equation of semi-odd order is of the form of a linear combination of $j_l(x)$ and $n_l(x)$, so that $V(x)$ is:

$$V(x) = Aj_l(x) + Bn_l(x) \tag{15}$$

Both $j_l(x)$ and $n_l(x)$ are solutions of the spherical Bessel equation of semi-odd order, and the expressions are shown below.

$$\begin{aligned} j_l(x) &= \sqrt{\frac{\pi}{2x}}J_{l+\frac{1}{2}}(x) \\ n_l(x) &= \sqrt{\frac{\pi}{2x}}N_{l+\frac{1}{2}}(x) \end{aligned} \tag{16}$$

For simplicity, $U(x)$ is indicated as:

$$U(x) = \frac{1}{i\omega\varepsilon r}\frac{\partial}{\partial x}(xH_\theta) = \frac{1}{i\omega\varepsilon r}\left(H_\theta + x\frac{\partial H_\theta}{\partial x}\right) = \frac{1}{i\omega\varepsilon r}[Aj_l(x) + Bn_l(x) + xAj_l'(x) + xBn_l'(x)] \tag{17}$$

In the meantime, $j'_l(x)$ and $n'_l(x)$ are the first order derivatives of the Bessel functions, and the corresponding equations are written as:

$$\begin{aligned} j_l'(x) &= \sqrt{\frac{\pi}{2x}}J'_{l+\frac{1}{2}}(x) - \frac{1}{2}\sqrt{\frac{\pi}{2}}x^{-\frac{3}{2}}J_{l+\frac{1}{2}}(x) \\ n_l'(x) &= \sqrt{\frac{\pi}{2x}}N'_{l+\frac{1}{2}}(x) - \frac{1}{2}\sqrt{\frac{\pi}{2}}x^{-\frac{3}{2}}N_{l+\frac{1}{2}}(x) \end{aligned} \tag{18}$$

In the following, the TMM is utilized to derive the expressions for the transmission properties of the 1D PSPCs. In similarity to the 1D planar non-magnetized plasma PCs, the vector $\left(\frac{V(x)}{U(x)}\right)$ is defined. Owing to the characteristics of the periodic arrangement of PCs, we are inspired to employ TMM to relate the corresponding vectors of different radii.

$$\begin{pmatrix} V(x) \\ U(x) \end{pmatrix} = \mathbf{M}\begin{pmatrix} V(x_0) \\ U(x_0) \end{pmatrix} = \begin{pmatrix} M_{11} & M_{12} \\ M_{21} & M_{22} \end{pmatrix}\begin{pmatrix} V(x_0) \\ U(x_0) \end{pmatrix} \tag{19}$$

The focus of the work now switches to solving for the elements in the matrix **M**. With the aim of making the calculation straightforward, the special values are taken and brought in.

$$\begin{aligned} V(x_0) &= 1 \\ U(x_0) &= 0 \end{aligned} \tag{20}$$

Next,

$$\begin{aligned} M_{11} = &\frac{j_l(x)}{j_l(x_0)n_l'(x_0) - n_l(x_0)j_l'(x_0)}\left[n_l'(x_0) + \frac{n_l(x_0)}{x_0}\right] \\ &+ \frac{n_l(x)}{n_l(x_0)j_l'(x_0) - n_l'(x_0)j_l(x_0)}\left[j_l'(x_0) + \frac{j_l(x_0)}{x_0}\right] \end{aligned} \tag{21}$$

$$\begin{aligned} M_{21} = \frac{1}{i\omega\varepsilon r}\Bigg\{ &\frac{j_l(x)}{j_l(x_0)n_l'(x_0) - n_l(x_0)j_l'(x_0)}\left[n_l'(x_0) + \frac{n_l(x_0)}{x_0}\right] \\ &+ \frac{n_l(x)}{n_l(x_0)j_l'(x_0) - n_l'(x_0)j_l(x_0)}\left[j_l'(x_0) + \frac{j_l(x_0)}{x_0}\right] \\ &+ \frac{xj_l'(x)}{j_l(x_0)n_l'(x_0) - n_l(x_0)j_l'(x_0)}\left[n_l{}'(x_0) + \frac{n_l(x_0)}{x_0}\right] \\ &+ \frac{xn_l'(x)}{n_l(x_0)j_l'(x_0) - n_l'(x_0)j_l(x_0)}\left[j_l'(x_0) + \frac{j_l(x_0)}{x_0}\right]\Bigg\} \end{aligned} \tag{22}$$

Similarly, assigning values to $V(x)$ and $U(x)$,

$$\begin{aligned} V(x_0) &= 0 \\ U(x_0) &= 1 \end{aligned} \tag{23}$$

M_{12} and M_{22} are further written as:

$$\begin{aligned} M_{12} = &\frac{j_l(x)}{n_l(x_0)j_l'(x_0) - n_l'(x_0)j_l(x_0)}\left[\frac{i\omega\varepsilon}{k}n_l(x_0)\right] \\ &+ \frac{n_l(x)}{j_l(x_0)n_l'(x_0) - n_l(x_0)j_l'(x_0)}\left[\frac{i\omega\varepsilon}{k}j_l(x_0)\right] \end{aligned} \tag{24}$$

$$\begin{aligned} M_{22} = \frac{1}{i\omega\varepsilon r}\Bigg\{ &\frac{j_l(x)}{n_l(x_0)j_l'(x_0) - n_l'(x_0)j_l(x_0)}\left[\frac{i\omega\varepsilon}{k}n_l(x_0)\right] \\ &+ \frac{n_l(x)}{j_l(x_0)n_l'(x_0) - n_l(x_0)j_l'(x_0)}\left[\frac{i\omega\varepsilon}{k}j_l(x_0)\right] \\ &+ \frac{xj_l'(x)}{n_l(x_0)j_l'(x_0) - n_l'(x_0)j_l(x_0)}\left[\frac{i\omega\varepsilon}{k}n_l(x_0)\right] \\ &+ \frac{xn_l{}'(x)}{j_l(x_0)n_l'(x_0) - n_l(x_0)j_l'(x_0)}\left[\frac{i\omega\varepsilon}{k}j_l(x_0)\right]\Bigg\} \end{aligned} \tag{25}$$

At this point, the matrix is derived. For wave propagation, the field can be expressed as a sum of two waves in opposite directions, which can be considered as a superposition of incident and outgoing waves. These two waves are usually represented by two Hankel functions:

$$\begin{aligned} h_1^{(1)}(x) &= j_l(x) + in_l(x) \\ h_1^{(2)}(x) &= j_l(x) - in_l(x) \end{aligned} \tag{26}$$

Taking into account the relationship between the electric and magnetic fields, the following defining equation can be adopted to demonstrate the propagation of electromagnetic waves.

$$\begin{aligned} C_l^{(2)}(x) &= 1 + x\frac{h_l^{(2)\prime}(x)}{h_l^{(2)}(x)} \\ C_l^{(1)}(x) &= 1 + x\frac{h_l^{(1)\prime}(x)}{h_l^{(1)}(x)} \end{aligned} \tag{27}$$

In 1D PSPCs, the evanescent spherical wave is incident at r_0 and exits at r_f. The reflection coefficient r_d and transmission coefficient t_d can be described by the elements in the transmission matrix **M**.

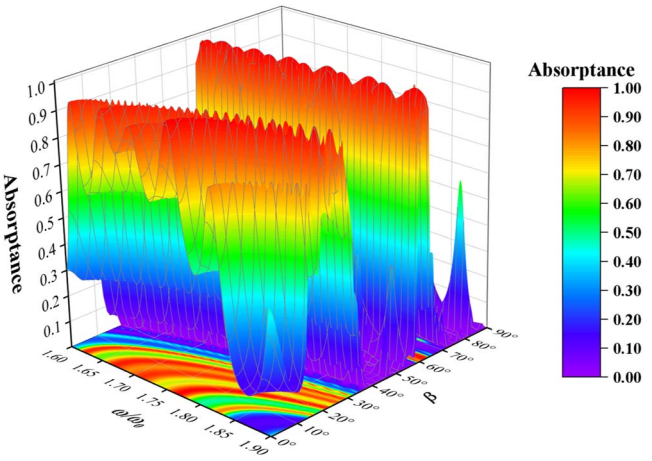

Figure 3. The absorption spectra of 1D PSPCs with Thue-Mores sequences in β variation with $d_Q = 0.2d$, $d_T = 0.25d$, $d_P = 0.55d$, $\omega_{p1} = 0.2\omega_0$ and $\nu_{c1} = 0.05\omega_{p1}$ in M_0 and $\omega_{p2} = 0.3\omega_0$ and $\nu_{c2} = 0.05\omega_{p2}$ in $\bar{M}_0$.

$$\begin{pmatrix} 1 + r_d \\ \dfrac{C_l^{(2)}(x_0)}{i\omega\varepsilon_0 r_0} + \dfrac{C_l^{(1)}(x_0)}{i\omega\varepsilon_0 r_0} r_d \end{pmatrix} = \mathbf{M}^{-1} \begin{pmatrix} t_d \\ \dfrac{C_l^{(2)}(x_f)}{i\omega\varepsilon_f r_f} t_d \end{pmatrix} \tag{28}$$

For the Thue-Morse sequence constructed in figure 1, M matrix is defined as:

$$\mathbf{M} = \mathbf{M_I M_H M_H M_I M_H M_I M_I M_H} \tag{29}$$

Further, it can be written as:

$$\mathbf{M} = \mathbf{M_P M_Q M_P M_T M_Q M_P M_T M_Q M_P M_Q M_P M_T M_Q M_P M_Q M_P M_Q M_P M_T M_Q} \tag{30}$$

$$\mathbf{M}^{-1} = \begin{pmatrix} M'_{11} & M'_{12} \\ M'_{21} & M'_{22} \end{pmatrix} \tag{31}$$

Substituting equations (21), (22), (24), and (25) into equations (28) and (29), the reflection coefficient r_d and transmission coefficient t_d can be expressed in terms of the elements in the transfer matrix **M**. The specific expression is written as:

$$t_d = \frac{C_l^{(1)}(x_0) - C_l^{(2)}(x_0)}{i\omega\varepsilon_0 r_0 \left[M_{11} \dfrac{C_l^{(1)}(x_0)}{i\omega\varepsilon_0 r_0} - M_{21} + \dfrac{C_l^{(2)}(x_f)}{i\omega\varepsilon_f r_f} \cdot \dfrac{C_l^{(1)}(x_0)}{i\omega\varepsilon_0 r_0} M_{12} - M_{22} \dfrac{C_l^{(2)}(x_f)}{i\omega\varepsilon_f r_f} \right]} \tag{32}$$

$$r_d = M_{11} + M_{12} \frac{C_l^{(2)}(x_f)}{i\omega\varepsilon_f r_f} \tag{33}$$

Ultimately get,

$$T = |t_d|^2 R = |r_d|^2 \tag{34}$$

$$A = 1 - T - R \tag{35}$$

3. Analysis and discussion

The 1D PSPCs with the Thue-Morse sequence is first analyzed. In the initial state (see figure 3), define normalized frequency $\omega_0 = 2\pi c/d$ and $\omega_c = 0$. At the same time make $r_0 = d = 1$, $d_Q = 0.2d$, $d_T = 0.25d$ and $d_P = 0.55d$. The plasma frequency is related to the imaginary part of the plasma, and to enhance the absorption bandwidth, $\omega_{p1} = 0.2\omega_0$ in M_0 and $\omega_{p2} = 0.3\omega_0$ in $\bar{M}_0$ are defined. The value of ν_c is related to ω_p, the initial case ordered $\nu_{c1} = 0.05\omega_{p1}$ in M_0 layer and $\nu_{c2} = 0.05\omega_{p2}$ in $\bar{M}_0$. If $\beta = 0$, four absorption bands can be clearly observed at the center frequencies of about $1.62\omega_0$, $1.67\omega_0$, $1.71\omega_0$, and $1.77\omega_0$ with absorption bandwidths (ABs) of $0.008\omega_0$, $0.017\omega_0$, $0.014\omega_0$, and $0.017\omega_0$, respectively. We also take notice that an ultra-wide AB appears between $\beta = 50°$~$60°$, and AB reaches a maximum of $0.154\omega_0$ with distinguished absorption characteristics.

The absorption spectra of the 1D PSPCs arranged with the Thue-Morse and Fibonacci sequences are presented in figure 4. Set $\omega_0 = 2\pi c/d$, $\omega_c = 0$, $r_0 = d = 1$, $d_Q = 0.2d$, $d_T = 0.25d$ and $d_P = 0.55d$. The plasma frequency is related to the imaginary part of the plasma, and to enhance the absorption bandwidth, $\omega_{p1} = 0.2\omega_0$ and $\nu_{c1} = 0.05\omega_{p1}$ in M_0 and $\omega_{p2} = 0.3\omega_0$ and $\nu_{c2} = 0.05\omega_{p2}$ in $\bar{M}_0$ are defined. The dashed line marks the part of

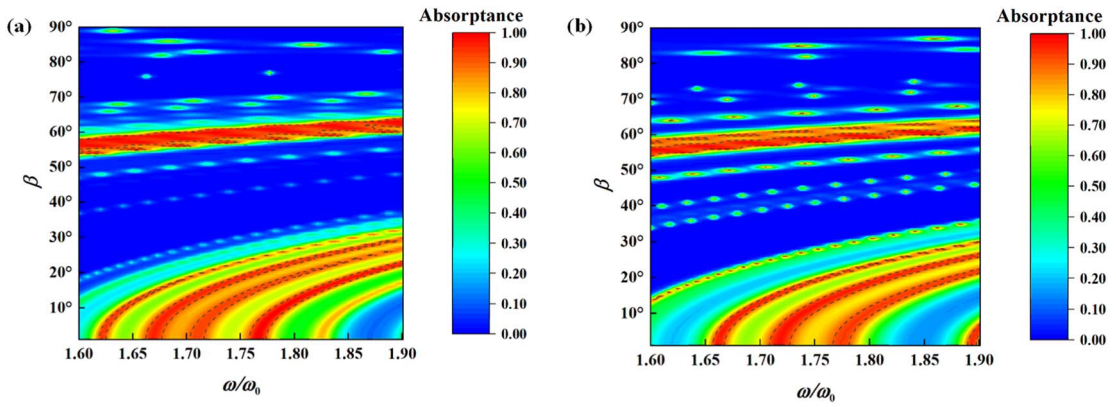

Figure 4. The influences of different arrangements on the absorption spectra, (a) Thue-Morse sequence and (b) Fibonacci sequence.

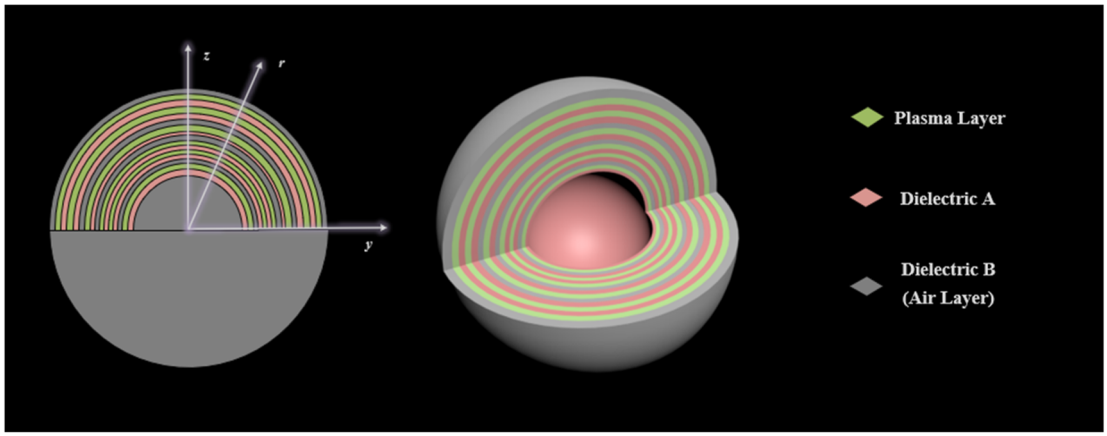

Figure 5. The structure of the 1D PSPCs arranged with the Fibonacci sequence.

the absorptance greater than 0.9. What is proposed above is the structure of 1D PSPCs (shown in figure 5) adapting 2-level Fibonacci sequence, with the specific arrangement (QPTQPQPTQPTQPTQPQPT) and $r_0 = d = 1$, $d_Q = 0.2d$, $d_T = 0.25d$ and $d_P = 0.55d$. The matrix $\mathbf{M_F}$ is written as:

$$\mathbf{M_F} = \mathbf{M_Q M_P M_T M_Q M_P M_T M_P M_T M_Q M_P M_T M_Q M_P M_Q M_P M_T} \tag{36}$$

And β, TE and TM waves are defined homoplastically to those in the Thue-Morse alignment.

From figure 4(b), it can be observed that the center frequency points of $1.66\omega_0$, $1.72\omega_0$, $1.77\omega_0$, and $1.89\omega_0$ emerge as ABs, but the bandwidth is diminutive, with a maximum of $0.018\omega_0$. Analogous to the 1D PSPCs of the Thue-Morse arrangement, they possess wide ABs at large angles, but the angular range is small, approximately 5°. The discrepancies in the absorption spectra are pertinent to the features of the sequence structure. The Thue-Morse sequence is generated through a series of element iterations in an akin way to the Fibonacci sequence. Hence, the PC structure constituted by the Thue-Morse sequence can be considered as a model linking the Fibonacci quasi-periodic PC structure to the periodic PC structure. Although the construction methods are semblable, the divergences in topology give rise to the differences in the electronic eigenstates. The electron eigenstates of the Thue-Morse sequence are exceeding disparate from the Fibonacci structure, revealing characteristics similar to Bloch waves and more localized. That is the reason why each absorption index of the Thue-Morse structure in figure 4 (a) is more preeminent than that of the Fibonacci structure in figure 4(b) [33]. Homogeneously, as seen in table 1, when $\beta = 0$, both sequences are capable of forming four ABs, but the bandwidths of the ABs are small, with a maximum value of only $0.018\omega_0$. When the angle is adjusted to $\beta = 60°$, the situation changes dramatically, and only one AB can be observed for both sequences. The bandwidth of the ABs in the Thue-Morse sequence reaches $0.154\omega_0$, much larger than the $0.04\omega_0$ in the Fibonacci sequence. Based on the above analysis, we can be convinced that favorable topological structures are indispensable conditions for the formation of wide ABs.

The effects of the change in ν_{c1} and ν_{c2} on the absorption spectra at $\beta = 0$, $r_0 = d = 1$, $d_Q = 0.2d$, $d_T = 0.25d$, $d_P = 0.55d$, $\omega_{p1} = 0.2\omega_0$ and $\omega_{p2} = 0.3\omega_0$ are plotted in figure 6. In particular, it is supplemented that the identical

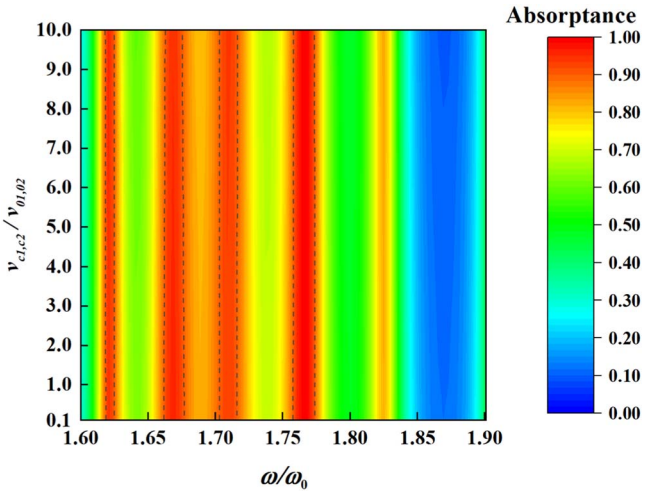

Figure 6. The absorption spectra of the 1D PSPCs arranged in Thue-Morse sequence under ν_{c1} and ν_{c2} variations ($\nu_{01} = 0.05\omega_{p1}$ and $\nu_{02} = 0.05\omega_{p2}$).

Table 1. Comparison of ABs of the 1D PSPCs with the Thue-Morse and Fibonacci sequences.

Structure	Thue-morse sequence		Fibonacci sequence	
Angel	Positions	Bandwidths	Positions	Bandwidths
	$1.618\omega_0 \sim 1.626\omega_0$	$0.008\omega_0$	$1.657\omega_0 \sim 1.668\omega_0$	$0.011\omega_0$
$\beta = 0$	$1.662\omega_0 \sim 1.678\omega_0$	$0.016\omega_0$	$1.709\omega_0 \sim 1.727\omega_0$	$0.018\omega_0$
	$1.703\omega_0 \sim 1.717\omega_0$	$0.014\omega_0$	$1.767\omega_0 \sim 1.782\omega_0$	$0.015\omega_0$
	$1.757\omega_0 \sim 1.774\omega_0$	$0.017\omega_0$	$1.889\omega_0 \sim 1.897\omega_0$	$0.008\omega_0$
$\beta = 60°$	Position	Bandwidth	Position	Bandwidth
	$1.712\omega_0 \sim 1.876\omega_0$	$0.154\omega_0$	$1.710\omega_0 \sim 1.750\omega_0$	$0.040\omega_0$

magnification of expansion is adopted here for both ν_{c1} and ν_{c2} to obtain a more pronounced phenomenon. When $\nu_{c1} = 0.05\omega_{p1}$ and $\nu_{c2} = 0.05\omega_{p2}$, the ABs appear in the frequency range near $1.62\omega_0$, $1.66\omega_0$, $1.72\omega_0$ and $1.77\omega_0$. When ν_{c1} and ν_{c2} continue to increase to 10 times the initial state, that is, $\nu_{c1} = 0.5\omega_{p1}$ and $\nu_{c2} = 0.5\omega_{p2}$, it can be readily easily noticed that the positions and bandwidths of ABs barely change. It shows that modifying ν_c does not cause conspicuous improvement in the absorption indexes, but only makes a slight increase in the amplitude of the absorption in the low absorptance regions, with little impact on the high absorptance.

Figure 7 draws the influences of altering r_0 on the absorption spectra for the case of $\beta = 60°$ with $d = 1$, $d_Q = 0.2d$, $d_T = 0.25d$, $d_P = 0.55d$, $\omega_{p1} = 0.2\omega_0$, $\nu_{c1} = 0.05\omega_{p1}$ $\omega_{p2} = 0.3\omega_0$, and $\nu_{c2} = 0.05\omega_{p2}$. When $r_0 = d$, the frequency range of AB reaches its maximum value of $0.15\omega_0$. Further increasing r_0 to $5d$, the original one AB at $r_0 = d$ splits into two, and the bandwidths decrease dramatically. When r_0 is greater than $5d$, a small portion of electromagnetic waves cannot be absorbed by the 1D PSPCs, and the absorpance is only about 0.8. When $r_0 = d$, due to the small initial radius, the dielectrics are arranged based on the Thue-Morse sequence to intercept any micro plane, which is supposed to be a curved surface with a large degree of bending. And r_0 continues to expand, the dielectric thicknesses have not transformed, so the plane taken in the case of large r_0 will be more analogous to the plane. The whittling of geometric superiority harms the absorption. Concurrently, if r_0 is small, the percentage of air in the spherical shell is at an extremely low level by comparison with the whole, so the small r_0 satisfies the requirement for 1D PSPCs to absorb electromagnetic waves and avoid their dissipation in the air. Therefore, it can be inferred that the appropriate r_0 is the key to forming distinguished ABs.

Comparing with figure 7, it can be found in figure 8 that when the incident angle varies, the frequency distribution of the absorbance over 0.9 part changes, but it still appears mainly in the part with small r_0.

The plasma frequency is one of the dominating indicators of plasma and is extraordinary closely bound up with the absorption indexes of 1D PSPCs. The air layer is used as a dividing line in the constructed structure, and the magnitude of the plasma frequency is set to ω_{p1} in the M_0 layer and ω_{p2} in the $\bar{M}_0$ layer. ω_{p1} is first analyzed in conjunction with figure 9 for the change in ω_{p1}.

The spectra of absorptance variation of ω_{p1} from $0.2\omega_0$ to $1.2\omega_0$ at $\beta = 60°$, $r_0 = d = 1$, $d_Q = 0.2d$, $d_T = 0.25d$, $d_P = 0.55d$, $\nu_{c1} = 0.05\omega_{p1}$ and $\nu_{c2} = 0.05\omega_{p2}$ are illustrated in figure 9. If ω_{p1} is between $0.2\omega_0 \sim 0.8\omega_0$, the 1D PSPCs generate an AB with a bandwidth of about $0.15\omega_0$. The enlargement in ω_{p1} only causes the AB to move toward the

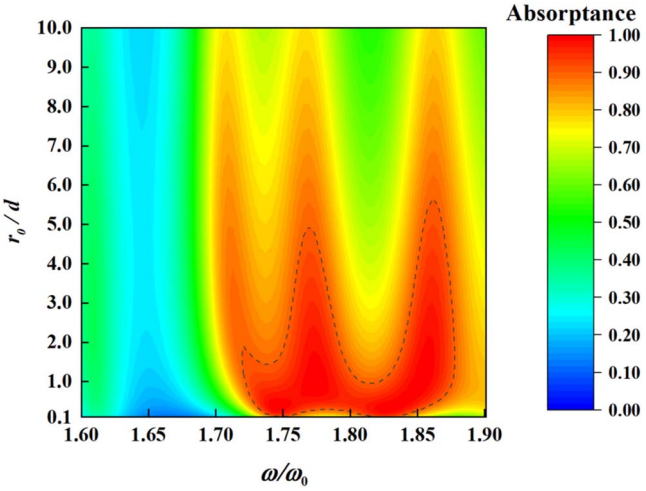

Figure 7. The absorptance of the 1D PSPCs while using the Thue-Morse sequence under r_0 adjustment and $\beta = 60°$, $d = 1$, $d_Q = 0.2d$, $d_T = 0.25d$, $d_P = 0.55d$, $\omega_{p1} = 0.2\omega_0$, $\nu_{c1} = 0.05\omega_{p1}$, $\omega_{p2} = 0.3\omega_0$ and $\nu_{c2} = 0.05\omega_{p2}$.

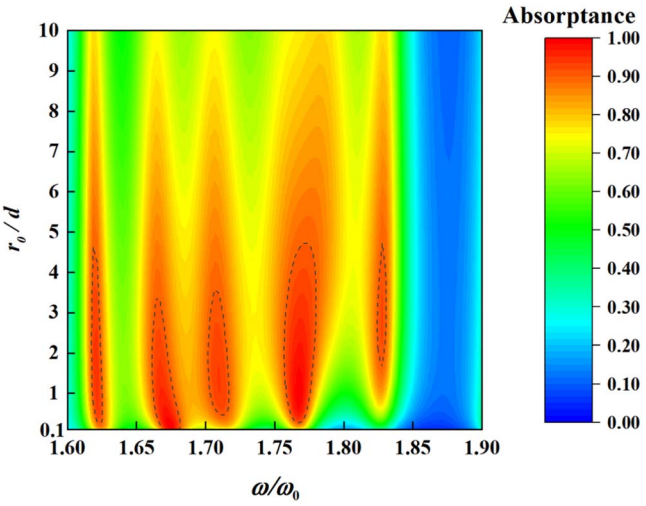

Figure 8. The absorptance of the 1D PSPCs while using the Thue-Morse sequence under r_0 adjustment and $\beta = 0$, $d = 1$, $d_Q = 0.2d$, $d_T = 0.25d$, $d_P = 0.55d$, $\omega_{p1} = 0.2\omega_0$, $\nu_{c1} = 0.05\omega_{p1}$, $\omega_{p2} = 0.3\omega_0$ and $\nu_{c2} = 0.05\omega_{p2}$.

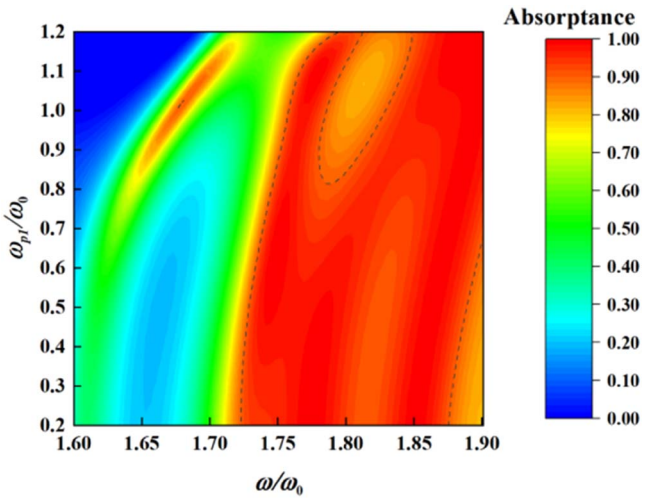

Figure 9. The effects of altering ω_{p1} on the ABs of 1D PSPCs aligned as the Thue-Morse sequences with $\beta = 60°$, $r_0 = d = 1$, $d_Q = 0.2d$, $d_T = 0.25d$, $d_P = 0.55d$, $\omega_{p1} = 0.2\omega_0$, $\nu_{c1} = 0.05\omega_{p1}$ and $\nu_{c2} = 0.05\omega_{p2}$.

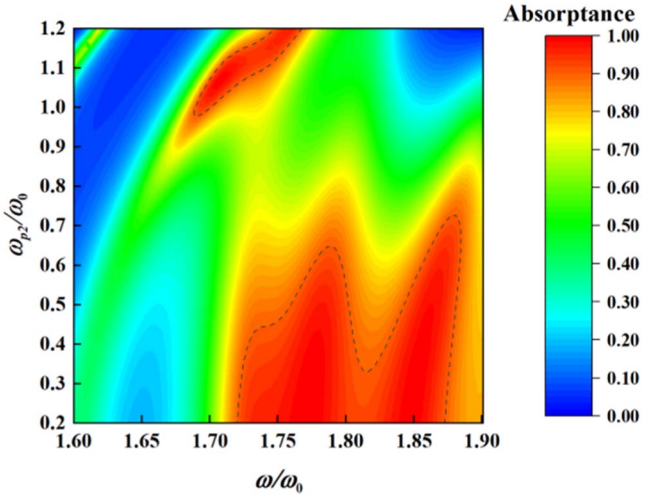

Figure 10. The effects of varying ω_{p2} on the 1D PSPCs ABs with Thue-Morse arrangement at $\beta = 60°$, $r_0 = d = 1$, $d_Q = 0.2d$, $d_T = 0.25d$, $d_P = 0.55d$, $\omega_{p2} = 0.3\omega_0$, $\nu_{c1} = 0.05\omega_{p1}$ and $\nu_{c2} = 0.05\omega_{p2}$.

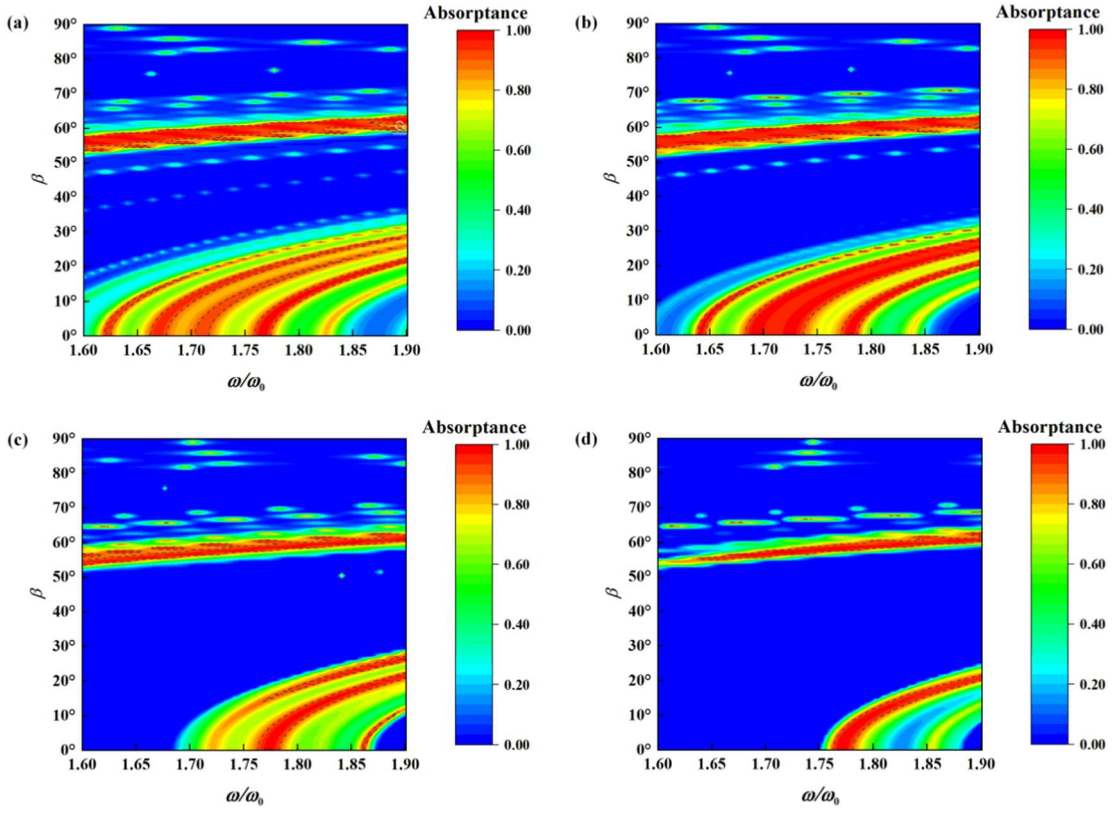

Figure 11. The absorption spectra for the 1D PSPCs adopting Thue-Morse alignment with different ω_{p1}, (a) $\omega_{p1} = 0.2\omega_0$ and $\omega_{p2} = 0.3\omega_0$, (b) $\omega_{p1} = 0.6\omega_0$ and $\omega_{p2} = 0.3\omega_0$, (c) $\omega_{p1} = \omega_0$ and $\omega_{p2} = 0.3\omega_0$, and (d) $\omega_{p1} = 1.2\omega_0$ and $\omega_{p2} = 0.3\omega_0$.

high frequencies, and there is no significant improvement in bandwidth. This is because the plasma frequency boost is essentially a modification of the imaginary part of the plasma, which in turn is a function of frequency, and therefore the ABs move toward the high-frequency region. After ω_{p1} amplifies to $0.8\omega_0$, the primordial AB breaks up into two ABs. In the meantime, A new narrow AB arises in the frequency range of $1.65\omega_0 \sim 1.70\omega_0$.

Figure 10 shows the absorption spectra of ω_{p2} varying from $0.2\omega_0$ to $1.2\omega_0$ for the premise of $\beta = 60°$, $r_0 = d = 1$, $d_Q = 0.2d$, $d_T = 0.25d$, $d_P = 0.55d$, $\nu_{c1} = 0.05\omega_{p1}$ and $\nu_{c2} = 0.05\omega_{p2}$. It can be conveniently observed that in the case of ω_{p2} between $0.2\omega_0 \sim 0.3\omega_0$, the 1D PSPCs possess a whole ultra-wide AB. Continuing to dilate ω_{p2}, a trend similar to that of ω_{p2} emerges, where the bandwidth of the ultra-wide AB becomes narrower and splits into two ABs. Until ω_{p2} increases to $0.7\omega_0$, there is no AB in the absorption spectra. similarly, in the case of ω_{p2} located in the interval $0.9\omega_0 \sim 1.2\omega_0$ interval a new AB is formed, occupying the region with the frequency of $1.65\omega_0 \sim 1.75\omega_0$.

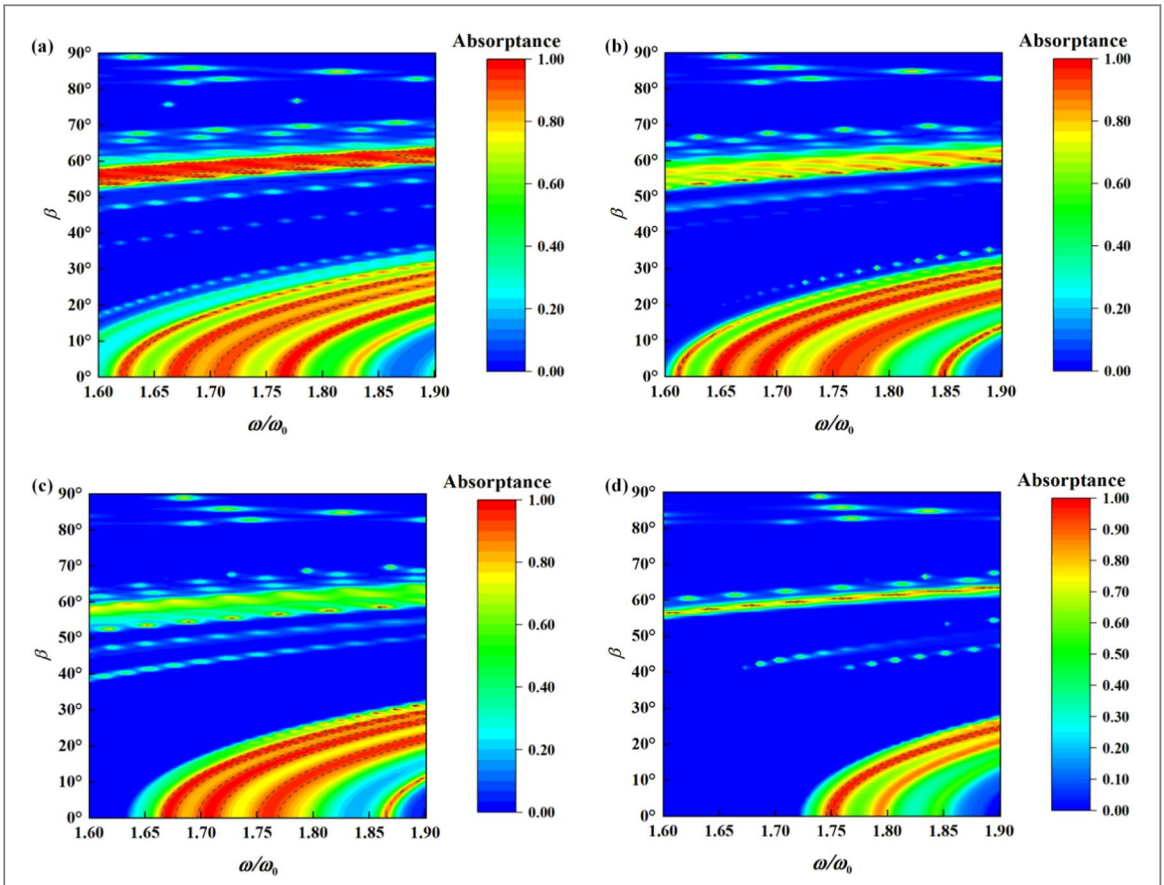

Figure 12. The absorption spectra of the 1D PSPCs at different ω_{p2} using Thue-Morse alignment, (a) $\omega_{p1} = 0.2\omega_0$ and $\omega_{p2} = 0.3\omega_0$, (b) $\omega_{p1} = 0.2\omega_0$ and $\omega_{p2} = 0.6\omega_0$, (c) $\omega_{p1} = 0.2\omega_0$ and $\omega_{p2} = 0.9\omega_0$, and (a) $\omega_{p1} = 0.2\omega_0$ and $\omega_{p2} = 1.2\omega_0$.

The effects of β on the absorption spectra are taken into account below. Figure 11(b) shows the distribution of ABs around $1.64\omega_0$, $1.71\omega_0$, and $1.78\omega_0$ for $\omega_{p1} = 0.6\omega_0$, where the maximum bandwidth is $0.054\omega_0$. Compared with figure 11(a), in the small β case, the enlargement of ω_{p1} brings an enhancement in the bandwidth of ABs, but the angular stability is reduced and the range in which ABs appear is narrowed. When $\omega_{p1} = \omega_0$, two ABs are observed to be generated at $1.76\omega_0$ and $1.86\omega_0$ for the case of $\beta = 0$. If $\omega_{p1} = 1.2\omega_0$, only one AB appears for $\beta = 0$ with a central frequency of $1.77\omega_0$. It is not toilless to infer that a further expansion in ω_{p1} makes the 1D PSPCs.

Modifying ω_{p2} also plays a momentous role in absorption. When $\beta = 0$, according to the results in figure 12(b), we can understand that there are ABs at frequencies $1.64\omega_0$, $1.68\omega_0$, $1.75\omega_0$, and $1.84\omega_0$, respectively. Compared with figure 12(a), the number of ABs elevates, but the AB at large β vanishes. Further extending ω_{p2}, it is found that the absorption characteristics recede at small β. Both the bandwidth and number of ABs decrease, and also the angular stability lowers, and the ultra-wide ABs occurring between $\beta = 50°\sim60°$ at $\omega_{p2} = 0.3\omega_0$ disappear. Setting ω_p with a gradient effectively enriches the plasma material so that the absorptance can remain high at large β. The frequency region corresponding to the ABs can be modulated by adjusting ω_p according to the actual physical scenarios.

4. Conclusion

In this work, firstly, the electric field expressions and magnetic field expressions in 1D PSPCs are obtained from the set of Maxwell's equations adopting the solution method of the spherical Bessel equations. The expressions and TMM are bonded to obtain the expressions for the absorptance in the 1D PSPCs under non-magnetization conditions. Meanwhile, based on the theoretical treatment of the 1D PSPCs, a quasi-periodic 1D PSPCs structure with a Thue-Morse arrangement is designed. And ω_p with gradient is set with the purpose of enriching the plasma material and obtaining a wide AB at a large β. A detailed discussion is then conducted on the factors that have an impact on ABs. Different topologies have a substantial impact on the distribution of ABs, and the dominating difference lies in the range of β covered by wide ABs and the locations and bandwidths of ABs in the case of small β. The changes in r_0 and ν_c are different from those of the structure. An expansion in r_0 causes a

decrease in the amplitude of the absorptance, and enlargement in ν_c causes an increase in the amplitude in the frequency region other than ABs. But both have almost no effect on ABs in terms of frequency. ω_p is an extraordinarily crucial indicator in plasma. Through analysis, it is revealed that ω_p is authoritative in the frequency distribution and angular stability of ABs, and proper ω_p is indispensable to the formation of ultra-wide ABs. The structure has important implications for the absorbers and also provides new research and development train of thought for the design of antenna protection devices, which have colossal potential.

Acknowledgments

This work was supported by the College Student Innovation Training Program of Nanjing University of Posts and Telecommunications.

Data availability statement

The data cannot be made publicly available upon publication because they are not available in a format that is sufficiently accessible or reusable by other researchers. The data that support the findings of this study are available upon reasonable request from the authors.

ORCID iDs

Haifeng Zhang https://orcid.org/0000-0002-9890-8345

References

[1] Yablonovitch E 1987 Inhibited spontaneous emission in solid-state physics and electronics *Phys. Rev. Lett.* **58** 2059
[2] John S 1987 Strong localization of photons in certain disordered dielectric super lattices *Phys. Rev. Lett.* **58** 2486
[3] Arnold K P, Halimi S I, Allen J A, Hu S and Weiss S M 2022 Photonic crystals with split ring unit cells for subwavelength light confinement *Opt. Lett.* **47** 661
[4] Liu Y, Chen W, Zhang W, Ma C Q, Chen H X, Xiong Y F, Yuan R, Tang J, Chen P and Hu W 2022 Visible and online detection of near-infrared optical vortices via nonlinear photonic crystals *Adv. Opt. Mater.* **10** 2101098
[5] Kim T *et al* 2022 Self-powered finger motion-sensing structural color display enabled by block copolymer photonic crystal *Nano Energy* **92** 106688
[6] Zhao Y J, Song N F, Gao F Y, Xu X B, Liu J Q and Liu C C 2021 Coherent perfect absorbers: time-reversed lasers *Opt. Express* **29** 32453
[7] Parandin F and Sheykhian A 2022 Design and simulation of a 2 × 1 All-Optical multiplexer based on photonic crystals *Opt. Laser Technol.* **151** 108021
[8] Pendry J B and MacKinnon A 1992 Two-dimensional photonic band structure in the chiral medium-transfer matrix method *Phys. Rev. Lett.* **69** 2772
[9] Jin C J, Qin B, Yang M and Qin R H 1997 Coherent perfect absorbers: time-reversed lasers *Opt. Commun.* **142** 179
[10] Li Z Y and Lin L L 2003 Photonic band structures solved by a plane-wave-based transfer-matrix method *Phys. Rev. E* **67** 046607
[11] Jiang Y and Hacker J 1994 Cylindrical-wave reflection and antireflection at media interfaces *Appl. Opt.* **33** 7431
[12] Jiang Y and Hacker J 1993 Distributed-Bragg reflectors and 90° couplers for cylindrical wave devices *Appl. Phys. Lett.* **63** 1453
[13] El-Naggar S A 2017 Optical guidance in cylindrical photonic crystals *Optik* **130** 584
[14] Larsen T, Bjarklev A, Hermann D and Broeng J 2003 Optical devices based on liquid crystal photonic bandgap fibres *Opt. Express* **11** 2589
[15] Zhang J T, Rao S S and Zhang H F 2022 Multiphysics sensor based on the nonreciprocal evanescent wave in the magnetized plasma cylindrical photonic crystals *IEEE Sens. J.* **22** 10500
[16] Santiago X G, Hammerschmidt M, Burger S, Rockstuhl C, Fernandez-Corbaton I and Zschiedrich L 2019 Decomposition of scattered electromagnetic fields into vector spherical wave functions on surfaces with general shapes *Phys. Rev. E* **99** 045406
[17] Moreira W L, Neves A A R, Garbos M K, Euser T G and Cesar C L 2010 Expansion of arbitrary electromagnetic fields in terms of vector spherical wave functions *Opt. Express* **24** 2370
[18] Yadav A, Danesh M, Zhong L B, Cheng J G, Jiang L and Chi L F 2016 Spectral plasmonic effect in the nano-cavity of dye-doped nanosphere-based photonic crystals *Nanotechnology* **27** 165703
[19] Xu B G, Zhang D G, Wang Y, Hong B B, Shu G X and He W L 2022 Characterization of Millimeter Wave Photonic Crystal Circulator with A Ferrite Sphere *Results Phys.* **34** 105315
[20] Lin Y S, Hung Y, Lin H Y, Tseng Y H, Chen Y F and Mou C Y 2007 Photonic crystals from monodisperse lanthanide-hydroxide-at-silica core/shell colloidal spheres *Adv. Mater.* **19** 577
[21] Li L, Li J R, Meng T T, Liu Z F, Zhou H, Zhu J and Shi J Q 2021 Diethylamine fluorescence sensor based on silica hollow sphere photonic crystals *Anal. Methods* **13** 2189
[22] Hojo H and Mase A 2004 Dispersion relation of electromagnetic waves in one-dimensional plasma photonic crystals *J. Plasma Fusion Res.* **80** 89
[23] Qi L M, Yang Z Q, Lan F, Gao X and Shi Z J 2021 Properties of obliquely incident electromagnetic wave in one-dimensional magnetized plasma photonic crystals *Phys. Plasmas* **17** 042501
[24] Dong C, Zheng Y, Shen K S, Liu H C, Xia S Q, Zhang J, Lu H, Zhang X Z and Liu Y F 2021 Polarization-independent wide-angle flexible multiband thermal emitters enabled by layered quasi-periodic photonic crystal *Opt. Laser Technol.* **156** 108474
[25] Voloch-Bloch N, Davidovich T, Ellenbogen T, Ganany-Padowicz A and Arie A 2010 Omnidirectional phase matching of arbitrary processes by radial quasi-periodic nonlinear photonic crystal *Opt. Lett.* **35** 2499

[26] Wu F, Chen M Y and Xiao S Y 2022 Wide-angle polarization selectivity based on anomalous defect mode in photonic crystal containing hyperbolic metamaterials *Opt. Lett.* **47** 2153
[27] Bikbaev R G, Vetrov S Y and Timofeev I V 2019 Epsilon-Near-Zero Absorber by Tamm Plasmon Polariton *Photonics* **6** 28
[28] Wu F, Wu X H, Xiao X Y, Liu G H and Li H J 2021 Broadband wide-angle multilayer absorber based on a broadband omnidirectional optical Tamm state *Opt. Express* **29** 23976
[29] Wu J 2022 TPP-assisted multi-band absorption enhancement in graphene based on Fibonacci quasiperiodic photonic crystal *Results Phys.* **33** 105210
[30] Wang Q Y, Wang P X, Wan B F and Zhang H F 2021 Investigation on the nonreciprocal properties of one-dimensional cylindrical magnetized plasma photonic crystals *J. Opt. Soc. Am. A* **38** 897
[31] Bicknel M 1975 A primer on the Thue-Morse sequence and related sequences *Fibonacci Quart.* **13** 345
[32] Ma Y, Zhang H, Zhang H F, Liu T and Li W Y 2018 Nonreciprocal properties of one-dimensional magnetized plasma photonic crystals with Fibonacci sequence *Plasma Sci. Technol.* **21** 015001
[33] Jiang X Y, Zhang Y G, Feng S L, Huang K C, Yi Y and Joannopoulos J D 2005 Photonic band gaps and localization in the Thue–Morse structures *Appl. Phys. Lett.* **86** 201110